

AD-A091 044

MARYLAND UNIV COLLEGE PARK COMPUTER SCIENCE CENTER
FITTING RANDOM FIELD MODELS TO IMAGES.(U)

F/G 5/8

AUG 80 R CHELLAPPA

AFOSR-77-3271

UNCLASSIFIED

CSC-TR-928

AFOSR-TR-80-1037

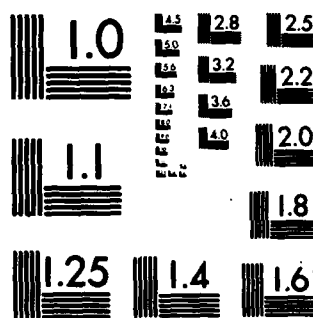
NL

END

DATE

12-83

DTIC

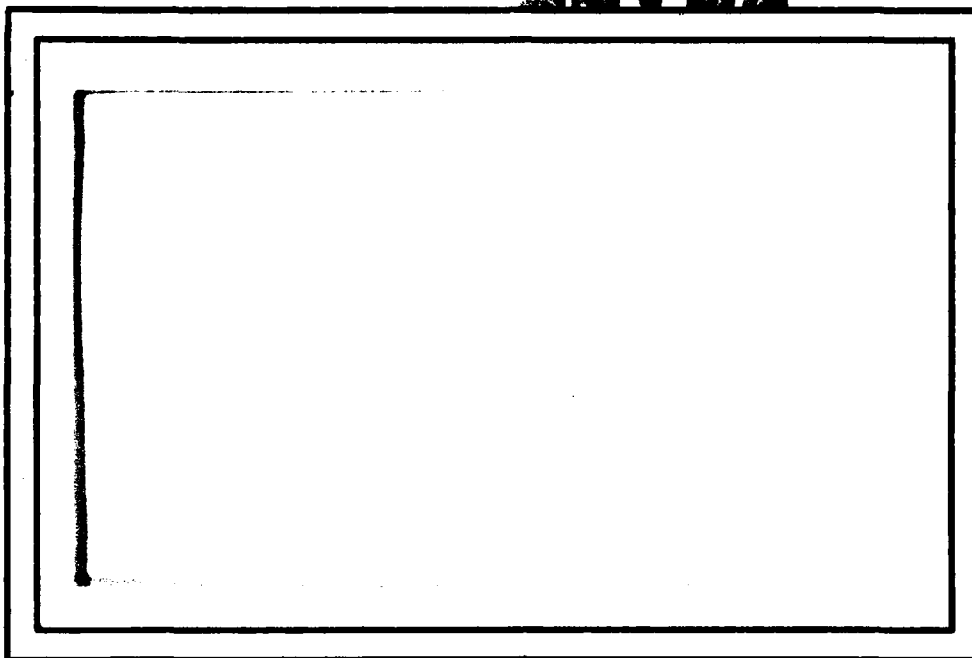


MICROCOPY RESOLUTION TEST CHART
NATIONAL BUREAU OF STANDARDS-1963-A

LEVEL II

12

AD A091044



DTIC
ELECTE
OCT 31 1980
S D
E

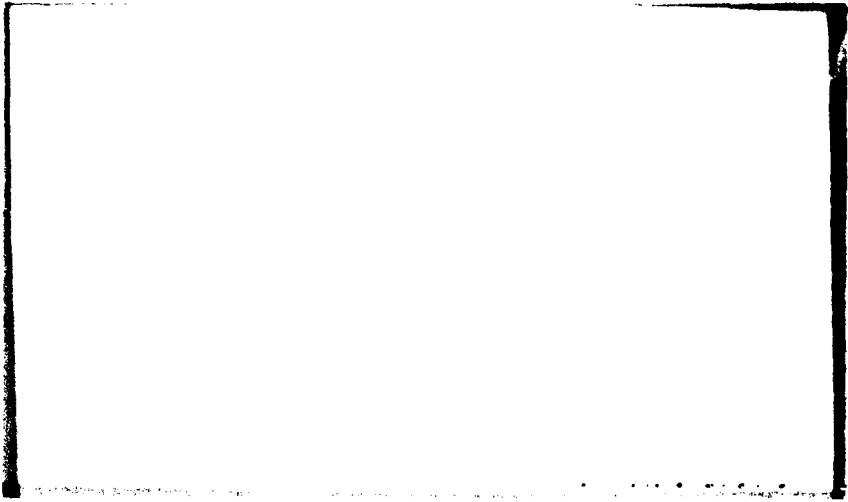
UNIVERSITY OF MARYLAND
COMPUTER SCIENCE CENTER

COLLEGE PARK, MARYLAND
20742

DDC FILE COPY

Approved for public release;
distribution unlimited.

80 10 21 039



AIR FORCE OFFICE OF SCIENTIFIC RESEARCH (AFSC)
NOTICE OF TRANSMITTAL TO DDC
This technical report has been reviewed and is
approved for public release IAW AFR 190-12 (7b).
Distribution is unlimited.

A. D. BLOSE
Technical Information Officer

TR-928 ✓
AFOSR-77-3271 ,

August, 1980

FITTING RANDOM FIELD MODELS TO IMAGES

R. Chellappa

Computer Vision Laboratory
Computer Science Center
University of Maryland
College Park, MD 20742

DTIC
S
E

ABSTRACT

↓
This paper deals with fitting two-dimensional stationary random field (RF) models to images. We assume that the given image is represented on a torus lattice, obeying an R.F. model driven by uncorrelated noise. The stochastic model is characterized by a set of unknown parameters. We describe two sets of experimental results. First, by assigning values to parameters in the stationary range, two-dimensional patterns are generated. It appears that quite a variety of patterns can be generated. Next we consider the problem of estimating the parameters, given an arbitrary image. By assuming a Gaussian structure for the noise, we given an iterative scheme to estimate the unknown parameters. We also implement a decision rule to choose an appropriate set of neighbors for the image. The theory is illustrated by applying it to synthetic patterns.
↑

The support of the U.S. Air Force Office of Scientific Research under Grant AFOSR-77-3271 is gratefully acknowledged, as is the help of Kathryn Riley in preparing this paper. The author is indebted to Profs. R. L. Kashyap and A. Rosenfeld for helpful discussions.

1. Introduction

Random field models have many applications in image processing and analysis; for instance, they can be used for the design of image enhancement or restoration algorithms [1-3], for image coding [4-6], and for characterization of textures [7-8]. Typically, an image is represented by two-dimensional scalar data, the gray level variations defined over a square grid. One of the important characteristics of such data is the statistical dependence of the gray levels within a neighbor set. For example, $y(i,j)$, the scalar gray level at position (i,j) , might be statistically dependent on the gray levels over a neighbor set that includes $\{(i-1,j), (i+1,j), (i,j-1), (i,j+1)\}$. This is in contrast to the familiar time series models where the dependence is strictly on the past observations.

Image models which include dependence in all directions (referred to as neighbor set models in the sequel) have been considered recently [3,6,7,8]. The neighbor set dependence might include the four nearest pixels (east, west, north, and south neighbors), the eight nearest pixels [3,8], or all the pixels inside a square window surrounding the pixel at (i,j) [6]. In these models, the observation $y(i,j)$ is written as a linear weighted sum of the observations over the corresponding neighbor set and an uncorrelated noise sequence and is characterized by a set of coefficients and the variance of the noise driving the model.

Prior to the use of these models, two problems have to be tackled, namely the estimation of the unknown parameters and the choice of an appropriate neighbor set for the given image. The second problem has received some attention in the literature [8-11]. The parameter estimation is usually handled by the maximum likelihood (ML) method. This involves imposing a Gaussian structure on the noise and deriving an expression for the likelihood of the observations. Unlike the cases of one-dimensional time series models or two-dimensional causal models, deriving an expression for the likelihood of the observations poses some difficulties for RF models. This is essentially due to the fact that the Jacobian of the transformation matrix from the noisy variates to the observations is not unity and is difficult to evaluate. Whittle [12] developed an asymptotic approximation for the determinant term, and developed approximate expressions for the likelihood function. Using spectral representation of the RF, likelihood functions in the transform domain were considered in [9,11]. The problem of evaluating the determinant can be avoided by making assumptions about the representation of the lattice. Specifically, by assuming representation on a torus lattice [8,10] (where the image is assumed to be folded over a torus), explicit expressions can be derived for the determinant term, as the transformation matrix possesses a block circulant structure whose eigenvalues can be written down explicitly. We use this torus representation developed in [8,10]

and write explicit expressions for the likelihood of the observations. Since the likelihood function is nonquadratic in the parameters, the estimates have to be determined by using numerical optimization procedures such as Newton-Raphson, etc. [13]. To save some computational effort, we suggest an iterative scheme, defined by using a logarithmic approximation to the determinant term. This method yields estimates that are close to ML estimates.

The second problem considered in fitting RF models is the choice of appropriate neighbors in images. From one-dimensional time series analysis it is known that the use of an appropriate model leads to good results in forecasting and similar applications. The problem of choice of appropriate neighbors has been considered in the literature [9,11]. The derivation of asymptotically consistent decision rules for the above problem is given in [11]; they are based on the corresponding decision rules for discriminating between different autoregressive models [14]. We implement this decision rule for choosing between different neighbor sets.

The usefulness of the estimation scheme and the decision rule for the choice of neighbors is demonstrated by applying them to synthetic patterns, the underlying true model of the synthetic pattern being known. This leads us to the problem of generating synthetic patterns. Computationally elegant

solutions using torus representations for generating synthetic patterns have been developed in [10]. We use this scheme and generate two-dimensional patterns. The patterns are quite varied and display the role played by the neighbor sets considered and the values of the coefficients.

The organization of the paper is as follows: In Section 2, we consider the estimation problem and develop an iterative method. The implementation of the decision rule for the choice of appropriate neighbors is also discussed. In Section 3, we give the experimental results. Discussion is presented in Section 4.

Accession For	
NTIS GRA&I	<input checked="checked" type="checkbox"/>
DDC TAB	<input type="checkbox"/>
Unannounced	<input type="checkbox"/>
Justification	
By _____	
Distribution/	
Availability Codes	
Dist.	Avail and/or special
A	

2. Estimation of parameters in RF models

Assume that the observations $y(i,j)$, $(i,j) \in \Omega$, have zero mean (which can be usually achieved by subtracting the sample mean from the original observations) and that $y(\cdot)$ obeys the RF model in (2.1), the neighbor set being denoted by N :

$$y(i,j) = \sum_{(k,\ell) \in N} \theta_{k,\ell} y((i,j)+(k,\ell)) + \sqrt{\rho} \omega(i,j), \quad (i,j) \in \Omega \quad (2.1)$$

In (2.1), (θ, ρ) are unknown parameters and $\omega(\cdot)$ is an i.i.d. noise sequence with zero mean and unit variance. Typically, the neighbor set N could include dependence on nearest neighbors in the north, east, south, and west directions, denoted as $\{(-1,0), (0,1), (1,0), (0,-1)\}$. To ensure stationarity, the coefficients $\{\theta_{k,\ell}, (k,\ell) \in N\}$ must obey

$$\left| \sum_{(k,\ell) \in N} \theta_{k,\ell} z_1^k z_2^\ell \right| < 1 \quad \text{whenever } |z_1| = |z_2| = 1 \quad (2.2)$$

Since we are working with a finite image, for an arbitrary neighbor set N , the neighbors of boundary pixels are not defined. Hence the image is assumed to be folded into a torus so that (2.3) is valid for all $(i,j) \in \Omega$:

$$y[(i,j)+(i_1,j_1)] = y[(i+i_1-1) \bmod M+1, (j+j_1-1) \bmod M+1] \quad (2.3)$$

The torus assumption ensures that all the relevant neighbors of any $y(s)$ belonging to the finite image are well defined.

Letting $\underline{y}^T = (y(1,1), \dots, y(1,M), \dots, y(M,M))$, $\underline{\omega}^T = (\omega(1,1), \dots, \omega(1,M), \dots, \omega(M,M))$, (2.1) can be rewritten as

$$B(\theta)y = \sqrt{\rho}\omega \quad (2.4)$$

where $B(\theta)$ is a block circulant transformation matrix from the noisy variates to the observations with a typical structure such as

$$B(\theta) = \begin{bmatrix} B_{1,1} & B_{1,2} & \cdots & B_{1,M} \\ B_{1,M} & B_{1,1} & \cdots & B_{1,M-1} \\ \cdots & \cdots & \cdots & \cdots \\ B_{1,2} & \cdots & \cdots & B_{1,1} \end{bmatrix} \quad (2.5)$$

For instance when the neighbor set of dependence N is $\{(-1,0), (0,1), (1,0), (0,-1)\}$ we have

$$B_{1,1} = \text{circulant } (1, -\theta_{0,1,0}, \dots, -\theta_{0,-1})$$

$$B_{1,2} = \text{circulant } (-\theta_{1,0,0}, \dots, 0)$$

$$B_{1,M} = \text{circulant } (-\theta_{-1,0,0}, \dots, 0)$$

and

$$B_{1,j} = 0 \quad j \neq 1, 2, M$$

For notational convenience the sum over $(i,j) \in \Omega$ is simply denoted by Ω .

Given an image, our interest is to estimate the parameters characterizing the image. One of the popular methods of estimation is the classical least squares method. This method yields the estimates defined below:

$$\hat{\theta} = \text{Arg min}_{\theta \in M} \{J_1(\theta)\} \quad (2.6)$$

where

$$J_1(\theta) = \sum_{\Omega} (y(i,j) - \theta^T z(i,j))^2 \quad (2.7)$$

and $z^T(i,j) = \{y[(i,j)+(k,l)], (k,l) \in N\}$

By performing the minimization in (2.6) we have

$$\hat{\theta} = [\sum_{\Omega} z(i,j) z^T(i,j)]^{-1} (\sum_{\Omega} z(i,j) y(i,j)) \quad (2.8)$$

and

$$\hat{\rho} = \frac{1}{M^2} \sum_{\Omega} (y(i,j) - \hat{\theta}^T z(i,j))^2 \quad (2.9)$$

One of the drawbacks of this method is that in general $\hat{\theta}$ is not always consistent [12,15]. Another popular method of estimation is the maximum likelihood (ML) method which yields asymptotically consistent and efficient estimates. To obtain an expression for the log likelihood function, we impose a Gaussian structure on the noise sequence $\omega(\cdot)$. Using the Gaussian assumption, the likelihood of the observations can be written as

$$\ln p(y|\hat{\theta}, \rho) = \ln \det B(\hat{\theta}) - (M^2/2) \ln 2\pi\rho - \frac{1}{2\rho} \sum_{\Omega} (y(i,j) - \hat{\theta}^T z(i,j))^2 \quad (2.10)$$

From [10], due to the block circulant structure of $B(\theta)$, we have

$$\det B(\hat{\theta}) = \prod_{\Omega} (1 - \hat{\theta}^T \psi_{ij}) \quad (2.11)$$

where

$$\psi_{ij} = \{\lambda_0^{k(i-1)+l(j-1)}, (k,l) \in N\}$$

and

$$\lambda_0 = \exp\{\sqrt{-1}2\pi/M\}$$

Using (2.11), we get

$$\ln p(\underline{y}|\underline{\theta}, \rho) = \sum_{\Omega} \ln(1 - \underline{\theta}^T \underline{\psi}_{ij}) - (M^2/2) \ln 2\pi\rho - \frac{1}{2\rho} \sum_{\Omega} (\underline{y}(i,j) - \underline{\theta}^T \underline{z}(i,j))^2 \quad (2.12)$$

To avoid computations involving complex quantities in (2.12), we use the following lemma.

Lemma 1:

$$\sum_{\Omega} \ln(1 - \underline{\theta}^T \underline{\psi}_{ij}) = 0.5 \sum_{\Omega} \ln(1 - 2\underline{\theta}^T \underline{C}_{ij} + \underline{\theta}^T \underline{Q}_{ij} \underline{\theta}) \quad (2.13)$$

where

$$\begin{aligned} \underline{C}_{ij}^T &= \{\cos[\lambda_0((i-1)k + (j-1)\ell)], (k, \ell) \in N\} \\ \underline{S}_{ij}^T &= \{\sin[\lambda_0((i-1)k + (j-1)\ell)], (k, \ell) \in N\} \end{aligned}$$

and

$$\underline{Q}_{ij} = \underline{C}_{ij} \underline{C}_{ij}^T + \underline{S}_{ij} \underline{S}_{ij}^T \quad (2.14)$$

Using Lemma 1, the likelihood function can be written as

$$\begin{aligned} \ln p(\underline{y}|\underline{\theta}, \rho) &= 0.5 \sum_{\Omega} \ln(1 - 2\underline{\theta}^T \underline{C}_{ij} + \underline{\theta}^T \underline{Q}_{ij} \underline{\theta}) \\ &\quad - (M^2/2) \ln 2\pi\rho - \frac{1}{2\rho} \sum_{\Omega} ((\underline{y}(i,j) - \underline{\theta}^T \underline{z}(i,j))^2 \end{aligned} \quad (2.15)$$

The ML estimates $\underline{\theta}^*$ and ρ^* are obtained by maximizing (2.15)

with respect to $\underline{\theta}$ and ρ and are given below:

$$\begin{aligned} \underline{\theta}^* &= \underset{\underline{\theta}}{\text{Arg min}} \{-0.5 \sum_{\Omega} \ln(1 - 2\underline{\theta}^T \underline{C}_{ij} + \underline{\theta}^T \underline{Q}_{ij} \underline{\theta}) \\ &\quad + (N/2) \ln \sum_{\Omega} (\underline{y}(i,j) - \underline{\theta}^T \underline{z}(i,j))^2 \end{aligned} \quad (2.16)$$

and

$$\rho^* = \frac{1}{M^2} \sum_{\Omega} (\underline{y}(i,j) - \underline{\theta}^{*T} \underline{z}(i,j))^2 \quad (2.17)$$

Since the log likelihood function is non-quadratic in θ , the estimation involves the use of numerical optimization methods such as Newton-Rophson [13] which are computationally expensive. We given an iterative method which yields estimates close to the ML estimates with a faster convergence rate. The estimation scheme is given by

Theorem 1: Let the observations $y(i,j), (i,j) \in \Omega$ obey the R.F. model in (2.1) characterized by θ, ρ . The estimates $\bar{\theta}, \bar{\rho}$ are given by the following iterative scheme:

$$\bar{\theta}_{t+1} = (\bar{R}_t - \frac{1}{\bar{\rho}_t} \bar{S})^{-1} (\bar{V} - \frac{1}{\bar{\rho}_t} \bar{U}_1) \quad (2.18)$$

and

$$\bar{\rho}_{t+1} = \frac{1}{M^2} \sum (y(i,j) - \bar{\theta}_{t+1}^T z(i,j))^2 \quad (2.19)$$

with

$$\bar{\theta}_0 = \bar{S}^{-1} \bar{U}_1$$

$$\bar{\rho}_0 = \frac{1}{M^2} \sum_{\Omega} (y(i,j) - \bar{\theta}_0^T z(i,j))^2$$

$$\bar{S} = \sum_{\Omega} z(i,j) z^T(i,j) \quad (2.20)$$

$$\bar{U}_1 = \sum_{\Omega} y(i,j) z(i,j) \quad (2.21)$$

$$\bar{V} = 0.5 \left(\sum \left(\frac{4}{a_{ij}} - \frac{2}{a_{ij}^2} \right) C_{ij} \right) \quad (2.22)$$

$$\bar{R} = 0.5 \left\{ \sum \left(\frac{2}{a_{ij}} - \frac{1}{a_{ij}^2} \right) Q_{ij} - \frac{2}{a_{ij}^2} C_{ij} C_{ij}^T \right\} \quad (2.23)$$

$$a_{ij} = 0.5 \{ [1 - 2 \bar{\theta}_t^T C_{ij} + \bar{\theta}_t^T Q_{ij} \bar{\theta}_t] \} \quad (2.24)$$

and

C_{ij} and Q_{ij} are as in Lemma 1.

The proof of Theorem 1 is given in the appendix.

Comments: (1) The iterative scheme is obtained by approximating the determinant term up to quadratic terms using a logarithmic approximation.

(2) Without losing much accuracy, further savings in computation can be achieved by letting $a_{ij} = a_t$, $1 \leq i, j \leq M$ where $a_t = \{\frac{1}{M^2} \sum_{ij} a_{ij}\}$. When this approximation is made, the vector V in (2.22) is identically equal to 0 (due to a property of sums of exponentials) and the following computational scheme results:

$$\bar{\theta}_{t+1} = -(\bar{R}_t - \frac{\bar{S}}{\rho_t}) (\frac{1}{\rho_t} U_1) \quad (2.25)$$

$$\bar{\rho}_{t+1} = \frac{1}{M^2} \sum (y(i,j) - \bar{\theta}_{t+1} z(i,j))^2 \quad (2.26)$$

where

$$\bar{R} = 0.5 \{ (\frac{2}{a_t} - \frac{1}{a_t^2}) \sum_{ij} Q_{ij} - \frac{2}{a_t} \sum_{ij} C_{ij} C_{ij}^T \} \quad (2.27)$$

and \bar{S} is as in (2.20).

We give a brief discussion regarding the decision rule for the choice of appropriate neighbor sets. Suppose we had three sets N_1 , N_2 , and N_3 of neighbors containing m_1 , m_2 , and m_3 neighbors, respectively. Corresponding to each N_i , we write the RF model as

$$y(i,j) = \sum_{(k,l) \in N_q} \theta_{q,k,l} y[(i,j)+(k,l)] + \sqrt{\rho_q} \omega(i,j) \quad (2.28)$$

$$\theta_{q,k,l} \neq 0 \quad (k,l) \in N_q, \quad q = 1,2,3$$

Then [8,10,11] the decision rule for the choice of appropriate neighbors is: choose the neighbor set N_{k^*} if

$$k^* = \arg \min_k \{C_k\} \quad \text{where} \\ C_k = \{-\sum_{\Omega} \ln(1-2\bar{\theta}^T C_{ij} + \bar{\theta}^T Q_{ij} \bar{\theta}) + M^2 \ln \rho + M_k \ln M^2\} \quad (2.29)$$

Suppose that we wish to also include unilateral or causal RF models; then the decision statistic C_k reduces to

$$C_k = M^2 \ln \bar{\rho} + M_k \ln M^2 \quad (2.30)$$

This follows from the fact that the Jacobian of the transformation matrix $B(\theta)$ from noisy variates to observations is unity [9,11]. Hence the model selection procedure consists of computing C_k for different models, depending on whether the underlying models are causal or noncausal, and choosing the one corresponding to the lowest C_k .

3. Experimental results

We describe the results of some experiments regarding the generation of two-dimensional patterns and estimation schemes developed in the previous section.

Experiment 1: Synthetic generation of two-dimensional patterns.

From (2.4) we have, for the observation set \underline{y} obeying an RF model,

$$B(\underline{\theta})\underline{y} = \sqrt{\rho}\underline{\omega} \quad (3.1)$$

The synthetic generation is then done by assigning some arbitrary values in the stationary region to $\underline{\theta}$ and ρ and using a pseudorandom number generator to form the vector $\underline{\omega}$. Since the matrix $B(\underline{\theta})$ has a block circulant structure, Fourier computations can be used for solving \underline{y} in (3.1) [10]. Before proceeding further, we need to define the following quantities: denote the M^2 Fourier vectors \underline{f}_{ij} , $1 \leq i, j \leq M$ by

$$\begin{aligned} \underline{f}_{ij} &= \text{column}(\underline{t}_j, \lambda_i \underline{t}_j, \dots, \lambda_i^{M-1} \underline{t}_j) \\ \underline{t}_j &= \text{column}(1, \lambda_j, \lambda_j^2, \dots, \lambda_j^{M-1}), \text{ M-vector} \\ \lambda_i &= \exp[\sqrt{-1} 2\pi(i-1)/M] \end{aligned}$$

The synthetic generation scheme then is as follows:

$$\underline{y} = \sum_{\Omega} (\underline{f}_{ij} \underline{x}_{ij} / \mu_{ij}) + \alpha \underline{1} \quad (3.2)$$

where

$$\underline{x}_{ij} = \frac{\sqrt{\rho}}{M^2} \sum_{\Omega} \underline{f}_{ij}^{*T} \underline{\omega}$$

and

$$\mu_{ij} = (1 - \underline{\theta}^T \underline{\psi}_{ij}), \quad 1 \leq i, j \leq M$$

We generate the vector ω from pseudorandom numbers, generate its Fourier sequence $\{x_{ij}\}$ by a two-dimensional FFT, and finally use (3.2). 16 such 64x64 images were generated using RF models with different neighbor sets and parameters. The gray scale values of the images were corrected to lie in the range 0-63. The details of the models are given in Table 1 and the corresponding images are shown in Fig. 1. It can be seen that the patterns generated are quite varied and some of them look similar to real textures. Contrary to the existing [16] belief that autoregressive RF models are incapable of exhibiting the local pattern replication attribute considered an essential ingredient of texture, some of the windows do exhibit repetitive patterns.

We use matrix notation in referring to windows of images. The (1,1) image illustrates the idea that causal models are also capable of accounting for some periodic patterns. The parabolic neighbor set seems to induce vertically oriented patterns in the (1,2) image. The (1,3) and (1,4) windows have identical parameter values but correspond to neighbor sets that are related (nearly a mirror reflection) and result in similar diagonal patterns but oriented differently.

Diagonal neighbors seem to induce diagonal patterns as in the (2,2), (3,4), (4,1), (4,3), and (4,4) windows. The windows in Fig. 1 are only typical examples and more interesting patterns could be generated by varying the neighbor sets and parameters.

Experiment 2: The role of parameter values in the structure of patterns.

To illustrate the role played by the coefficients in generating the two-dimensional patterns, we consider the pattern corresponding to the RF model $N = \{(-1,1), (1,1), (1,-1), (-1,-1)\}$, $\alpha = 30.000$, $\rho = 1.1111$ and $\theta_{-1,1} = \theta_{1,-1} = -.14$ and $\theta_{1,1} = \theta_{-1,-1} = .28$. The values of the parameters tried are given in Table 2 and the corresponding pictures in Fig. 2. Note that as the parameters are varied the basic pattern is still retained but the "busyness" of the pattern is varied. Also note that by changing the sign of the diagonal weights, diagonal patterns of opposite orientation are produced. All the patterns considered thus far were generated using the same pseudorandom number generator. The role played by using different sets of pseudorandom numbers is illustrated later.

Experiment 3: To test the usefulness of the estimation scheme and the choice of appropriate neighbor sets, experiments were done with two synthetic patterns. The true model corresponding to the first pattern is defined as follows: the values of α and ρ are 30 and 1.1111 respectively, the neighbor set $N = \{(-1,0), (-1,1), (1,1), (1,0), (1,-1), (-1,-1)\}$, and $\theta_{-1,0} = \theta_{1,0} = .12$, $\theta_{-1,1} = \theta_{1,-1} = .28$, $\theta_{1,1} = \theta_{-1,-1} = -.14$. Using the model, the synthetic image (1,1) in Fig. 3 was generated. But for correct inference purposes regarding the estimation schemes, the original

window (values not scaled for display purposes) was used. For estimation of the parameters, the sample mean of the window was subtracted and the iterative scheme developed in (2.25-2.27) was used for different RF models. The test statistic C_k defined in (2.29) or (2.30) was also computed. The actual values of the estimates corresponding to different neighbor sets are given in Table 3 and the corresponding reconstructed images are given in Fig. 3.

Table 3 shows that the estimated values corresponding to the true neighbor set are close to the true values. The so-called least square estimates corresponding to the true neighbor set are inefficient compared to the estimates obtained by the scheme developed here. Note that when extra neighbors are added, the corresponding parameter values are very small. The decision statistics corresponding to the models considered are tabulated in Table 4 and the decision rule picks up the true model.

Fig. 3 shows the pictures corresponding to the different neighbor sets using an identical array of noise variables in Table 3. The (1,2) window corresponding to the least square estimate of the true model is a poor reproduction of the original in (1,1). On the other hand, the (1,3) window corresponding to the approximate ML estimates developed here is very close

to the original. The reproductions corresponding to neighbor sets $\{(-1,0), (1,0), (0,-1)\}$ and $\{(-1,0), (0,1), (1,0), (0,-1)\}$ are very poor. The windows (2,4), (3,1), and (3,2) look close to the originals as the corresponding models include the original neighbor set. But the decision rule suggested here correctly eliminates these models.

Since in real world applications the procedure of using identical noise variables for the reconstructed pictures as for the originals is unrealistic, the natural question is how sensitive are these patterns to different sequences of noise variables. To answer this question synthetic generation of patterns were done using different random number sequences and the true model as in Expt. 3, but with estimated parameters. The resulting patterns are shown in Fig. 4. Note that the variations in the patterns are noticeable if one takes a close look, but the basic patterns are retained in all the windows. (Window (1,3) corresponds to the random numbers used in Fig. 3 and consequently is identical to window (1,3) of Fig. 3.)

Table 5 and Fig. 5 correspond to experiments with the synthetic pattern generated by the causal model $\{(-1,0), (0,-1), (-1,-1)\}$ with $\alpha = 30.8870$, $\rho = 0.1087$, $\theta_{-1,0} = .9704$, $\theta_{0,-1} = .9735$ and $\theta_{-1,-1} = -.9686$. The estimates corresponding to different RF models are given in Table 5. While estimating the parameters for causal models the least square estimates themselves were treated as the approximate ML estimates, though the

underlying patterns were produced using a torus structure. (The error in approximation due to the torus representation used for the causal models is negligible.) Note that the decision rule (see Table 6 for the test statistics) picks up correctly the causal model compared to other noncausal models. This shows that it is not true that noncausal models are always superior to causal models.

Fig. 5 shows the windows constructed using the models in Table 5. The quality of reproduction using the causal model is markedly superior to that using the semicausal model $\{(1,4), (2,1)\}$ or noncausal model $(2,2)$. (In fact, the noncausal model $\{(-1,0), (0,1), (1,0), (0,-1)\}$ yielded estimates in the nonstationary range.) Since the extra neighbors used in the models corresponding to $(1,4)$ and $(2,1)$ have very small values these patterns look very similar. As more and more noncausal members are added (windows $(3,1)$ and $(3,2)$) the reproduction is somewhat better. Windows $(2,3)$ and $(2,4)$ correspond to causal neighbor sets that include the original model and hence the quality of reconstruction is good.

The variations produced in the pattern corresponding to different random number sequences (considered in Fig. 4) are shown in Fig. 6. Note that the basic patterns are retained.

4. Discussion

We have considered the problem of estimating the unknown parameters of an RF model and the choice of appropriate neighbors. The iterative estimation scheme yields estimates that are close to the ML estimates. The problem of statistical inference of stationary RF models has been previously considered by Whittle [12] and Larimore [9]. Since in [12] representation on a square lattice was used, the evaluation of the determinant of the transformation matrix is difficult, and approximate methods using power series expansion of the spectral density were used. The computation of the determinant can be conveniently done in the transform domain as in [9], but the method involves the assumption that the Fourier transforms of $y(\cdot)$ are uncorrelated, which is true only for an infinite image. By using the torus representation for finite images, as done in this paper, the determinant can be explicitly evaluated and the exact likelihood function can be written down. This leads to computations in the spatial domain as against the transform domain.

The iterative scheme suggested here yields estimates that are close to the true parameters, with less computational effort compared to numerical optimization methods such as Newton-Raphson, etc.

We have also implemented a decision rule for the choice of neighbors which correctly picks up the true model against many competing models.

To illustrate that RF models are indeed capable of generating a wide variety of patterns, examples of synthetic generation results have been presented. Most of the patterns possess the local pattern replication property which is considered to be an essential ingredient of textures.

We have illustrated the theory using synthetic patterns. Currently, work is under progress in testing the estimation scheme with real textures.

References

1. A. Habibi, "Two-dimensional Bayesian estimate of images", Proc. IEEE, Vol. 60, pp. 878-883, July 1972.
2. D. P. Panda and A. C. Kak, "Recursive least squares smoothing of noise in images", IEEE Trans. on Acoustics, Speech and Signal Processing, Vol. ASSP-25, pp. 520-524, Dec. 1977.
3. A. K. Jain and J. R. Jain, "Partial difference equations and finite difference methods in image processing--part 2: image restoration", IEEE Trans. on Automatic Control, Vol. AC-23, pp. 817-833, Oct. 1978.
4. E. J. Delp, R. L. Kashyap and O. R. Mitchell, "Image data compression using autoregressive time series models", Pattern Recognition, Vol. 11, pp. 313-323, Dec. 1979.
5. A. K. Jain and E. Angel, "Image restoration, modeling and reduction of dimensionality", IEEE Trans. on Computers, Vol. C-23, pp. 470-476, May 1976.
6. K. Deguchi and I. Morishita, "Image coding and reconstruction by two-dimensional optimal linear estimation", Proc. 4th IJCPR, pp. 530-532, Nov. 1978.
7. J. T. Tou, "Pictorial feature extraction and recognition via image modeling", Computer Graphics Image Processing, Vol. 12, pp. 376-406, April 1980.
8. R. L. Kashyap, "Univariate and multivariate random field models for images", Computer Graphics Image Processing, Vol. 12, pp. 257-370, March 1980.
9. W. E. Larimore, "Statistical inference on stationary random fields", Proc. IEEE, Vol. 65, pp. 961-970, June 1977.
10. R. L. Kashyap, "Random field models on torus lattices for finite images" (submitted).
11. R. L. Kashyap, R. Chellappa, and N. Ahuja, "Decision rules for choice of neighbors in random field models of images" (to appear in Computer Graphics Image Processing).
12. P. Whittle, "On stationary processes in the plane", Biometrika, Vol. 41, pp. 434-449, 1954.

13. N. K. Gupta and R. K. Mehra, "Computational aspects of maximum likelihood estimation and reduction in sensitivity function calculations", IEEE Trans. on Automatic Control, Vol. AC-19, pp. 774-783, Dec. 1974.
14. R. L. Kashyap, "A Bayesian comparison of different classes of dynamic models using empirical data", IEEE Trans. on Automatic Control, Vol. AC-22, pp. 715-727, Oct. 1977.
15. R. L. Kashyap and R. Chellappa, "Estimation methods for random field models of images" (in preparation).
16. J. W. Modestino, "Texture discrimination based upon an assumed stochastic texture model", TR-79-3, Electrical and Systems Engineering Dept., Rensselaer Polytechnic Institute, Troy, New York, July 1979.

Appendix

Proof of Lemma 1:

From (2.11),

$$\ln \det B(\theta) = \sum_{\Omega} \ln(1 - \theta^T \tilde{\Psi}_{ij}) \quad (1)$$

Using the definition of $\tilde{\Psi}_{ij}$,

$$(1 - \theta^T \tilde{\Psi}_{ij}) = (1 - \theta^T \tilde{C}_{ij} - \sqrt{-1} \theta^T \tilde{S}_{ij}) \quad (2)$$

where

$$\tilde{C}_{ij}^T = \{\cos \lambda_0 [(i-1)k + (j-1)\ell], (k, \ell) \in N\}$$

and

$$\tilde{S}_{ij}^T = \{\sin \lambda_0 [(i-1)k + (j-1)\ell], (k, \ell) \in N\}$$

From (2),

$$\ln(1 - \theta^T \tilde{\Psi}_{ij}) = \frac{1}{2} \ln[(1 - \theta^T \tilde{C}_{ij})^2 + (\theta^T \tilde{S}_{ij})^2] + \tan^{-1} \left(\frac{-\theta^T \tilde{S}_{ij}}{1 - \theta^T \tilde{C}_{ij}} \right) \quad (3)$$

Since $\sum_{\Omega} \ln(1 - \theta^T \tilde{\Psi}_{ij})$ is real

$$\begin{aligned} \ln \det B(\theta) &= \sum_{\Omega} \ln(1 - \theta^T \tilde{\Psi}_{ij}) \\ &= 0.5 \left[\sum_{\Omega} \ln(1 + \theta^T (\tilde{C}_{ij} \tilde{C}_{ij}^T + \tilde{S}_{ij} \tilde{S}_{ij}^T) - 2\theta^T \tilde{C}_{ij}) \right] \quad (4) \end{aligned}$$

Defining

$$\tilde{Q}_{ij} = \tilde{C}_{ij} \tilde{C}_{ij}^T + \tilde{S}_{ij} \tilde{S}_{ij}^T$$

proves Lemma 1.

Proof of Theorem 1: Prior to proving Theorem 1 we need the following lemma which is proved subsequently.

Lemma 2:

$$\sum \ln(1 - \tilde{\theta}_{ij}^T \tilde{\psi}_{ij}) = K(a_{ij}) - \tilde{v}^T \tilde{\theta} + \tilde{\theta}^T R \tilde{\theta} \quad (5)$$

where the vector \tilde{v} and the matrix R are as in (2.22) and (2.23)

and

$$K(a_{ij}) = 0.5 \{ \sum \ln a_{ij} + (1 - a_{ij})/a_{ij} - (1 - a_{ij})/2a_{ij}^2 \}$$

From (2.15) and Lemma 2,

$$\begin{aligned} \ln p(\tilde{y} | \tilde{\theta}, \rho) &= K(a_{ij}) - \tilde{v}^T \tilde{\theta} + \tilde{\theta}^T R \tilde{\theta} - (M^2/2) \ln 2\pi\rho \\ &\quad - \frac{1}{2\rho} \sum_{\Omega} (y(i,j) - \tilde{\theta}^T z(i,j))^2 \end{aligned} \quad (6)$$

Differentiating w.r.t. $\tilde{\theta}$ and ρ and equating to zero,

$$-\tilde{v} + R\tilde{\theta} + \frac{1}{\rho} \sum_{\Omega} z(i,j) (y(i,j) - \tilde{\theta}^T z(i,j)) \tilde{\theta} = 0 \quad (7)$$

and

$$\bar{\rho} = \frac{1}{M^2} \sum_{\Omega} (y(i,j) - \tilde{\theta}^T z(i,j))^2 \quad (8)$$

Solving (7), and defining

$$\bar{S} = \sum_{\Omega} z(i,j) z^T(i,j), \quad (9)$$

$$\tilde{u}_1 = \sum_{\Omega} z(i,j) y(i,j) \quad (10)$$

we have

$$\tilde{\theta} = (R - \frac{1}{\rho} \bar{S})^{-1} (\tilde{v} - \frac{1}{\rho} \tilde{u}_1) \quad (11)$$

From (11) and (13) we obtain the following iterative scheme:

$$\tilde{\theta}_{t+1} = (\tilde{R} - \frac{1}{\hat{\rho}_t} \tilde{U}_1)^{-1} (\tilde{V} - \frac{1}{\hat{\rho}_t} \tilde{U}_1) \quad (12)$$

and

$$\tilde{\rho}_{t+1} = \frac{1}{M^2} \sum_{\Omega} (y(i,j) - \tilde{\theta}_{t+1}^T z(i,j))^2 \quad (13)$$

with

$$\tilde{\theta}_0 = \tilde{S}^{-1} \tilde{U}_1 \quad (14)$$

and

$$\hat{\rho}_0 = \frac{1}{M^2} \sum_{\Omega} (y(i,j) - \theta_0^T z(i,j))^2 \quad (15)$$

Proof of Lemma 2: Using the expansion,

$$\ln x = \ln a + \frac{x-a}{a} - \frac{1}{2a^2} (x-a)^2 \dots, \quad 0 < x \leq 2a$$

we have

$$\begin{aligned} \ln(1 + \tilde{\theta}_{ij}^T \tilde{Q}_{ij} \tilde{\theta} - 2\tilde{\theta}_{ij}^T \tilde{C}_{ij}) &= \ln a_{ij} + \\ &+ (1 - a_{ij} + \tilde{\theta}_{ij}^T \tilde{Q}_{ij} \tilde{\theta} - 2\tilde{\theta}_{ij}^T \tilde{C}_{ij}) / a_{ij} \\ &- (1 - a_{ij} + \tilde{\theta}_{ij}^T \tilde{Q}_{ij} \tilde{\theta} - 2\tilde{\theta}_{ij}^T \tilde{C}_{ij})^2 / 2a_{ij}^2 + \dots \end{aligned} \quad (16)$$

Taking the sum,

$$\sum \ln(1 + \tilde{\theta}_{ij}^T \tilde{Q}_{ij} \tilde{\theta} - 2\tilde{\theta}_{ij}^T \tilde{C}_{ij}) = \sum \ln a_{ij} + (1 - a_{ij}) / a_{ij} - (1 - a_{ij})^2 / 2a_{ij}^2$$

$$- \tilde{\theta}^T \sum_{\Omega} \left(\frac{4}{a_{ij}} - \frac{2}{a_{ij}^2} \right) \tilde{C}_{ij}$$

$$+ \tilde{\theta}^T \left(\sum_{\Omega} \left(\frac{2}{a_{ij}} - \frac{1}{a_{ij}^2} \right) \tilde{Q}_{ij} - \frac{2}{a_{ij}^2} \tilde{C}_{ij} \tilde{C}_{ij}^T \right) \tilde{\theta}$$

Defining

$$\tilde{V} = 0.5 \sum_{\Omega} \left(\frac{4}{a_{ij}} - \frac{2}{a_{ij}^2} \right) C_{ij}$$

and

$$\tilde{R} = 0.5 \sum_{\Omega} \left[\left(\frac{2}{a_{ij}} - \frac{1}{a_{ij}^2} \right) Q_{ij} - \frac{2}{a_{ij}^2} C_{ij} C_{ij}^T \right]$$

we arrive at Lemma 2.

NUMBER	NEIGHBOR SET	α	ρ	COEFFICIENTS
(1,1)	(-1,0), (0,-1), (-1,-1)	30.8870	0.1087	$\theta_{-1,0} = .9704$, $\theta_{0,-1} = .9735$, $\theta_{-1,-1} = -.9686$
(1,2)	(-1,0), (1,0), (0,-1)	30.000	1.1111	$\theta_{-1,0} = \theta_{1,0} = .18$, $\theta_{0,-1} = -.12$
(1,3)	(-1,0), (0,-1), (-1,-1), (1,-1)	30.000	1.1111	$\theta_{-1,0} = .18$, $\theta_{0,-1} = 0.1011$ $\theta_{-1,-1} = -1.0390$, $\theta_{1,-1} = -.1804$
(1,4)	(-1,0), (0,1), (1,1), (-1,1)	30.000	1.1111	$\theta_{-1,0} = .18$, $\theta_{0,-1} = 1.1011$ $\theta_{1,1} = -.1804$, $\theta_{-1,1} = -1.0390$
(2,1)	(-1,0), (0,1), (1,0), (0,-1)	30.000	1.1111	$\theta_{-1,0} = \theta_{1,0} = -.1200$ $\theta_{0,1} = \theta_{0,-1} = .2600$
(2,2)	(-1,1), (1,1) (1,-1), (-1,-1)	30.000	1.1111	$\theta_{-1,1} = \theta_{1,-1} = -.14$ $\theta_{1,1} = \theta_{-1,-1} = .28$
(2,3)	(0,1), (1,1), (1,0), (0,-1), (-1,0)	30.000	1.1111	$\theta_{0,1} = .12$, $\theta_{0,-1} = .15$, $\theta_{-1,0} = .18$ $\theta_{1,0} = .10$, $\theta_{1,1} = .11$
(2,4)	(-1,1), (0,1), (1,1) (1,-1), (0,-1), (-1,-1)	30.000	1.1111	$\theta_{-1,1} = \theta_{1,-1} = .23$, $\theta_{0,1} = \theta_{0,-1}$ $\theta_{1,1} = \theta_{-1,-1} = .22$ $= -.14$

Table 1. Details of RF models corresponding to Fig. 1.

NUMBER	NEIGHBOR SET	α	ρ	COEFFICIENTS
(3,1)	(0,1), (1,1), (1,0), (1,-1), (0,-1), (-1,-1), (-1,1), (-1,0)	30.000	1.111	$\theta_{0,1}=\theta_{0,-1}=.5081$ $\theta_{1,0}=\theta_{-1,0}=.5256$ $\theta_{1,1}=\theta_{-1,-1}=-.2874$ $\theta_{1,-1}=\theta_{-1,1}=-.2480$
(3,2)	(0,1), (0,-1), (-1,0), (1,0) (0,2), (0,-2), (-2,0), (2,0)	30.000	1.111	$\theta_{0,1}=\theta_{0,-1}=.20$ $\theta_{1,0}=\theta_{-1,0}=-.10$ $\theta_{0,2}=\theta_{0,-2}=-.15$ $\theta_{2,0}=\theta_{-2,0}=.20$
(3,3)	(0,1), (0,-1), (-1,0), (1,0)	30.000	1.111	$\theta_{0,1}=\theta_{0,-1}=.1825$ $\theta_{-1,0}=\theta_{1,0}=.3794$
(3,4)	(-1,0), (1,0), (0,-1), (0,1), (1,1), (-1,-1)	30.000	1.111	$\theta_{-1,0}=\theta_{1,0}=.18$ $\theta_{1,1}=\theta_{-1,-1}=.22$ $\theta_{0,1}=\theta_{0,-1}=-.10$
(4,1)	(-1,0), (1,0), (-1,-1), (1,1), (1,-1), (-1,1)	30.000	1.111	$\theta_{-1,0}=\theta_{1,0}=.12$ $\theta_{1,-1}=\theta_{-1,1}=.2800$ $\theta_{-1,-1}=\theta_{1,1}=-.1400$
(4,2)	(-1,0), (0,-1), (-1,-1), (-2,0), (0,-2)	30.000	1.111	$\theta_{-1,0}=1.0388$ $\theta_{0,-1}=.9046$ $\theta_{-1,-1}=-.7288$ $\theta_{-2,0}=-.1814$ $\theta_{0,-2}=-.1088$
(4,3)	(-1,0), (1,0), (0,-1), (0,1), (-1,1), (1,-1)	30.000	1.111	$\theta_{-1,0}=\theta_{1,0}=.28$ $\theta_{1,-1}=\theta_{-1,1}=.22$ $\theta_{0,-1}=\theta_{0,1}=-.14$
(4,4)	(0,1), (1,1), (1,0), (1,-1) (0,-1), (-1,-1), (-1,1) (-1,0)	30.000	1.111	$\theta_{0,1}=\theta_{0,-1}=.5246$ $\theta_{1,0}=\theta_{-1,0}=.5357$ $\theta_{1,1}=\theta_{-1,-1}=-.3126$ $\theta_{1,-1}=\theta_{-1,1}=-.2500$

Table 1 (cont'd.)

NUMBER	$\theta_{1,1} = \theta_{-1,-1}$	$\theta_{1,-1} = \theta_{-1,1}$
(1,1)	.28	-.14
(1,2)	.28	-.10
(1,3)	.28	-.06
(1,4)	.30	-.10
(2,1)	.32	-.10
(2,2)	.34	-.10
(2,3)	.36	-.10
(2,4)	.38	-.10
(3,1)	-.14	.28
(3,2)	-.10	.28
(3,3)	-.06	.28
(3,4)	-.10	.30
(4,1)	-.10	.32
(4,2)	-.10	.34
(4,3)	-.10	.36
(4,4)	-.10	.38

Table 2. Values of parameters used to illustrate the role played by them in synthesizing patterns.
 $\alpha = 30.00$, $\rho = 1.1111$, $N = \{(-1,1), (1,1), (1,-1), (-1,-1)\}$

NUMBER	NEIGHBOR SET	$\hat{\alpha}$	$\hat{\rho}$	COEFFICIENTS
(1,1)	$(-1,0), (-1,1),$ $(1,1), (1,0),$ $(1,-1), (-1,-1)$	30.000	1.1111	$\theta_{-1,0} = \theta_{1,0} = .12$ $\theta_{1,1} = \theta_{-1,-1} = -.14$ $\theta_{1,-1} = \theta_{-1,1} = .28$ (TRUE MODEL)
(1,2)	"	30.034	1.0126	$\theta_{-1,0} = \theta_{1,0} = .1470$ Least sq. estimate $\theta_{1,1} = \theta_{-1,-1} = -.1526$ correspond- ing to $\theta_{0,1} = \theta_{0,-1} = .3680$ true model
(1,3)	"	30.034	1.1240	$\theta_{-1,0} = \theta_{1,0} = .1119$ $\theta_{1,1} = \theta_{-1,-1} = -.1577$ \approx ML estimate $\theta_{1,-1} = \theta_{-1,1} = .2785$ correspond- ing to true model
(1,4)	$(-1,1), (1,-1),$ $(0,1), (0,-1),$ $(-1,-1), (1,1)$	30.034	1.2355	$\theta_{-1,1} = \theta_{1,-1} = .2871$ $\theta_{0,1} = \theta_{0,-1} = .0386$ $\theta_{-1,-1} = \theta_{1,1} = -.1641$
(2,1)	$(-1,0), (1,0), (0,-1)$	30.034	3.6432	$\theta_{-1,0} = .0582$ $\theta_{1,0} = .1609$ $\theta_{0,-1} = .0870$

Table 3. Details of models corresponding to Fig. 3.

NUMBER	NEIGHBOR SET	$\hat{\alpha}$	$\hat{\rho}$	COEFFICIENTS
(2,2)	(0,-1), (-1,0), (-1,-1)	30.034	2.5713	$\theta_{0,-1} = .0504$ $\theta_{-1,0} = .2826$ $\theta_{-1,-1} = -.5625$
(2,3)	(0,1), (0,-1), (-1,0), (1,0)	30.034	3.6463	$\theta_{0,1} = \theta_{0,-1} = .0369$ $\theta_{-1,0} = \theta_{1,0} = .1082$
(2,4)	(-1,1), (1,1), (1,-1), (-1,-1)	30.034	1.2421	$\theta_{-1,1} = \theta_{1,-1} = .2940$ $\theta_{1,1} = \theta_{-1,-1} = -.1605$
(3,1)	(0,1), (1,1), (1,0), (1,-1), (0,-1), (-1,-1), (-1,0)	30.034	1.1228	$\theta_{0,1} = \theta_{0,-1} = .0230$ $\theta_{1,0} = \theta_{-1,0} = .1090$ $\theta_{1,1} = \theta_{-1,-1} = -.1602$ $\theta_{1,-1} = \theta_{-1,1} = .2758$
(3,2)	(-1,0), (-1,1), (1,1), (1,0), (1,-1), (-1,-1), (-2,0), (0,-2)	30.034	1.1119	$\theta_{-1,0} = \theta_{1,0} = .1187$ $\theta_{1,1} = \theta_{-1,-1} = -.1478$ $\theta_{-1,1} = \theta_{1,-1} = .2783$ $\theta_{-2,0} = \theta_{2,0} = -.0281$

Table 3 (cont'd.)

NUMBER	TEST STATISTIC	
(1,3)	1852.052	+ True model
(1,4)	2196.110	
(2,1)	5397.05	
(2,2)	3893.3	
(2,3)	5440.82	
(2,4)	2221.6	
(3,1)	1874.0	
(3,2)	1939.7	

Table 4. Test statistics corresponding to the models in Table 2.

NUMBER	NEIGHBOR SET	$\hat{\alpha}$	$\hat{\rho}$	COEFFICIENTS
(1,1)	$(-1,0), (0,-1), (-1,-1)$	30.8870	.1087	$\theta_{-1,0} = .9704$ $\theta_{0,-1} = .9735$ $\theta_{-1,-1} = -.9686$ TRUE MODEL
(1,2)	$(-1,0), (0,-1), (-1,-1)$	31.096	0.1136	$\theta_{-1,0} = .9772$ $\theta_{0,-1} = .9798$ $\theta_{-1,-1} = -.9790$
(1,3)	$(-1,0), (1,0), (0,-1)$	31.096	2.2604	$\theta_{-1,0} = .2172$ $\theta_{1,0} = .2675$ $\theta_{0,-1} = .4763$
(1,4)	$(-1,0), (0,-1), (-1,-1), (0,1)$	31.096	1.1443	$\theta_{-1,0} = .9904$ $\theta_{1,0} = .00006$ $\theta_{0,-1} = .9905$ $\theta_{-1,-1} = -.9997$
(2,1)	$(-1,0), (0,-1), (-1,-1), (0,1)$	31.096	1.1462	$\theta_{-1,0} = .9912$ $\theta_{0,-1} = .9915$ $\theta_{-1,-1} = -1.0007$ $\theta_{0,1} = -.0011$

Table 5. Details of models corresponding to Fig. 3.

NUMBER	NEIGHBOR SET	$\hat{\alpha}$	$\hat{\rho}$	COEFFICIENTS
(2,2)	(0,1), (0,-1), (-1,0), (1,0)	31.096		$\theta_{0,1} = \theta_{0,-1} = .2245$ $\theta_{-1,0} = \theta_{1,0} = .2812$ Model is nonstationary
(2,3)	(0,-1), (-1,0) (-1,-1), (-2,-2)	31.096	1.1314	$\theta_{0,-1} = .9800$ $\theta_{-1,0} = .9772$ $\theta_{-1,-1} = -.9784$ $\theta_{-2,-2} = -.0015$
(2,4)	(0,-1), (-1,0), (-1,-1), (-2,0), (0,-2)	31.096	1.1313	$\theta_{0,-1} = .9770$ $\theta_{-1,0} = .9820$ $\theta_{-1,-1} = -.9794$ $\theta_{-2,0} = .00079$ $\theta_{0,2} = -.002818$
(3,1)	(-1,0), (1,0), (0,-1), (0,1), (1,1), (-1,-1)	31.096	.0574	$\theta_{-1,0} = \theta_{1,0} = .4903$ $\theta_{0,-1} = \theta_{0,1} = .4916$ $\theta_{1,1} = \theta_{-1,-1} = -.4908$
(3,2)	(0,1), (1,1), (1,0), (1,-1), (0,-1), (-1,-1), (-1,0), (-1,1)	31.096	.0307	$\theta_{0,1} = \theta_{0,-1} = .4990$ $\theta_{-1,0} = \theta_{1,0} = .4984$ $\theta_{1,1} = \theta_{-1,-1} = .2505$ $\theta_{1,-1} = \theta_{-1,1} = -.2472$

Table 5 (cont'd.)

NUMBER	TEST STATISTIC
(1,2)	-8900.0
(1,3)	3883.16
(1,4)	-8663.66
(2,1)	-8657.67
(2,2)	-- (non-stationary)
(2,3)	-8892.0
(2,4)	-8884.6
(3,1)	-6102.58
(3,2)	-6866.006

Table 6. Test statistics corresponding to the models in Figure 3.

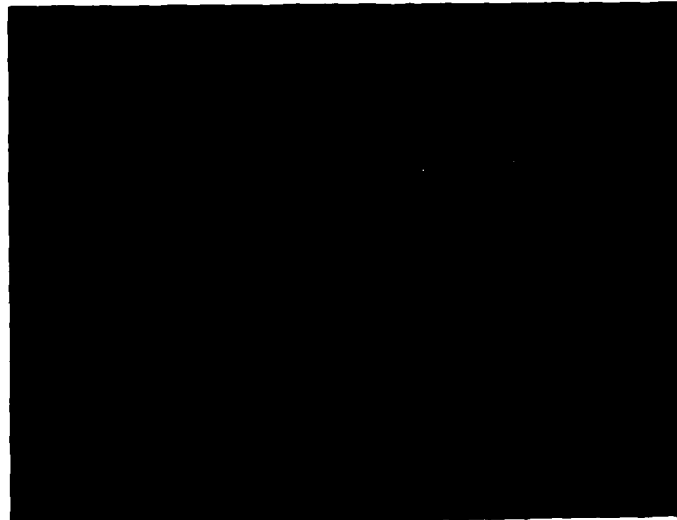


Figure 1. Examples of synthetic generation of images using RF models (see Table 1).



Figure 2. Patterns produced by models with the same neighbor set $N=\{(-1,1), (1,1), (1,-1), (-1,-1)\}$, $\alpha=30.034$, $\rho=1.1240$ but with different sets of values for the coefficients (see Table 2).



Figure 3. Reconstruction of images corresponding to the true model $N=\{(-1,0), (-1,1), (1,1), (1,0), (1,-1), (-1,-1)\}$. See Table 3 for details.



Figure 4. Patterns produced using different sequences of random numbers and the model $N=\{(-1,0), (-1,1), (1,1), (1,0), (1,-1), (-1,-1)\}$ with $\alpha=30.034$, $\rho=1.1240$ and $\theta_{-1,0}=\theta_{1,0}=.1119$, $\theta_{-1,1}=\theta_{1,-1}=.2785$, $\theta_{1,1}=\theta_{-1,-1}=-.1577$.



Figure 5. Reconstruction of images corresponding to the true model $N=\{(-1,0),(0,-1),(-1,-1)\}$. See Table 5 for details.



Figure 6. Patterns produced using different sequences of random numbers and the model $N=\{(-1,0),(0,-1),(-1,-1)\}$, $\alpha=31.096$, $\rho=0.1136$, $\theta_{-1,0}=.9772$, $\theta_{0,-1}=.9798$, $\theta_{-1,-1}=-.9790$.

UNCLASSIFIED

SECURITY CLASSIFICATION OF THIS PAGE (When Data Entered)

REPORT DOCUMENTATION PAGE		READ INSTRUCTIONS BEFORE COMPLETING FORM
1. REPORT NUMBER (18) AFOSR-TR-80-1037	2. GOVT ACCESSION NO. AD-A092	3. RECIPIENT'S CATALOG NUMBER 044
4. TITLE (and Subtitle) (6) FITTING RANDOM FIELD MODELS TO IMAGES.		5. TYPE OF REPORT & PERIOD COVERED (9) Interim Repts
7. AUTHOR(s) (10) R./Chellappa		6. PERFORMING ORG. REPORT NUMBER
(14) 200-TR-928		8. CONTRACT OR GRANT NUMBER(s) (15) AFOSR-77-3271
9. PERFORMING ORGANIZATION NAME AND ADDRESS University of Maryland Computer Science Center College Park, Maryland 20742 (13) 432		10. PROGRAM ELEMENT, PROJECT, TASK AREA & WORK UNIT NUMBERS 61102F (16) 2304A2 (17) A26
11. CONTROLLING OFFICE NAME AND ADDRESS Air Force Office of Scientific Research/NM Bolling AFB, Washington, DC 20332		12. REPORT DATE August 1980
14. MONITORING AGENCY NAME & ADDRESS (If different from Controlling Office) (11) AFB		13. NUMBER OF PAGES 41
		15. SECURITY CLASS. (of this report) UNCLASSIFIED
16. DISTRIBUTION STATEMENT (of this Report) Approved for public release; distribution unlimited.		15a. DECLASSIFICATION/DOWNGRADING SCHEDULE
17. DISTRIBUTION STATEMENT (of the abstract entered in Block 20, if different from Report)		
18. SUPPLEMENTARY NOTES		
19. KEY WORDS (Continue on reverse side if necessary and identify by block number)		
20. ABSTRACT (Continue on reverse side if necessary and identify by block number) This paper deals with fitting two-dimensional stationary random field (RF) models to images. We assume that the given image is represented on a torus lattice, obeying an R. F. model driven by <u>uncorrelated noise</u> . The stochastic model is characterized imtal results. First, by assigning values to parameters in the stationary range, two-dimensional patterns are generated. It appears that quite a variety of patterns can be generated. Next we consider the problem of estimating the parameters, given an arbitrary image. By assuming a Gaussian structure for the noise, we given implement a decision		

DD FORM 1473 1 JAN 73 EDITION OF 1 NOV 65 IS OBSOLETE

UNCLASSIFIED

403028

SECURITY CLASSIFICATION OF THIS PAGE (When Data Entered)

UNCLASSIFIED

SECURITY CLASSIFICATION OF THIS PAGE(When Data Entered)

rule to choose an appropriate set of neighbors for the image. The theory is illustrated by applying it to synthetic patterns.

UNCLASSIFIED